IEEJ Journal of Industry Applications
Vol.11 No.2 pp.317–326 DOI: 10.1541/ieejjia.21005712

Paper

Effect of Harmonic Current Suppression on Iron Loss of IPMSM Using Repetitive Perfect Tracking Control

Yuhiro Inagaki* Student Member, Masahiro Mae* Student Member
Osamu Shimizu* Member, Sakahisa Nagai* Member
Hiroshi Fujimoto* Senior Member, Takayuki Miyajima** Member
Yoshiki Yasuda** Member, Akio Yamagiwa** Member

(Manuscript received May 20, 2021, revised Sep. 30, 2021)
J-STAGE Advance published date : Nov. 26, 2021

Permanent magnet synchronous motors (PMSMs) have wide applicability owing to their many advantages. For efficient driving of PMSMs, a number of high-efficiency control methods have been developed. However, few studies have discussed the relationship between the tracking characteristics to the current command and driving loss. Here, we propose using the RPTC, which is a digital controller with high tracking performance, as the current controller for reducing the iron loss. The RPTC can suppress the periodic disturbances; therefore, the iron loss caused by the harmonic current in the input current is reduced. Simulations confirmed that the presence or absence of the harmonic current affects the iron loss reduction. Experiments also showed that RPTC reduced the extent of the iron loss in interior permanent magnet synchronous motors (IPMSMs).

Keywords: IPMSM, iron loss, harmonic current suppression, repetitive perfect tracking control

1. Introduction

Permanent magnet synchronous motors (PMSMs) have many advantages, such as high output power and controllability, and are widely used in industrial applications. In particular, interior permanent magnet synchronous motors (IPMSMs) are often used in electric vehicles, owing to their large torque. For further effective utilization of energy, it is necessary to drive PMSMs with high efficiency through control.

Analyzing the causes of driving loss and taking relevant measures to alleviate it is important for achieving highly efficient motor driving. For PMSMs, the loss is mainly classified into copper loss and iron loss. Copper loss occurs in the motor windings, while iron loss occurs in the electromagnetic steel sheet. Typical examples of highly efficient current control are the $i_d = 0$ control and maximum torque per ampere (MTPA) control [1]. These methodologies reduce copper loss. However, these are not necessarily the most efficient control methods, because they do not consider iron loss. Some methods that determine the dq-axis current command, minimizing the sum of copper loss and iron loss, have also been proposed [2]–[4]. However, the tracking performance of current command often depends on the general current PI controller, and only a few studies examined the effect of changing the current controller on the motor efficiency.

IPMSMs exhibit large harmonics, owing to their structural issues such as the shape and placement of the magnets [5]; these harmonics deteriorate the tracking performance with respect to the current command. In addition, the tracking error caused by the harmonic current increases iron loss and reduces the overall motor's driving efficiency. Therefore, it is important to suppress the harmonic current for an efficient IPMSM drive. Because the harmonic current can be regarded as a periodic disturbance, control methods such as repetitive control are effective in suppressing it. In particular, RPTC, corresponding to a repetitive control based on perfect tracking control (PTC) [6]–[8] can be expected to strongly suppress the harmonic current and achieve high tracking performance with respect to the current command, by applying it as the current controller.

In this study, the effect of suppressing the harmonic current on the motor's iron loss was validated by comparing the iron loss results for the dq-axis current control of an IPMSM with those for a PI controller only and for an RPTC. The validation was based on simulations and experiments.

2. Iron Loss of PMSM

2.1 Causes of Iron Loss Iron loss occurs in the iron core of a PMSM and is broadly classified into hysteresis loss and eddy current loss [9]. The IPMSM core contains harmonic magnetic flux density components owing to various factors, such as harmonic currents. Several iron loss model equations and experimental phenomena, such as minor loops of hysteresis, show that iron loss is affected by an increase in the presence of higher-frequency components [10]–[12].

Electromagnetic simulations were conducted to confirm the effect of the harmonic current on iron loss. In addition,

* The University of Tokyo
5-1-5, Kashiwanoha, Kashiwa, Chiba 227-8561, Japan
** DAIKIN INDUSTRIES, Ltd.
1-1-1, Nishi-Hitotsuya, Settsu, Osaka 566-8585, Japan

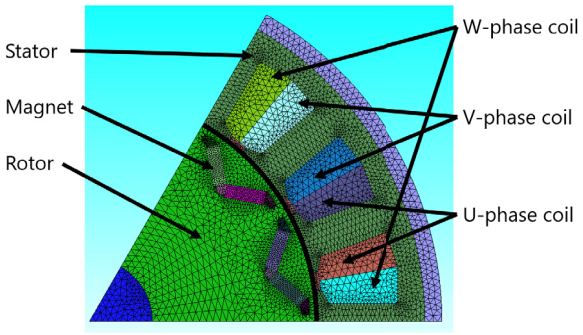

Fig. 1. Simulated IPMSM model (1/6 model (60°))

Table 1. Parameters of the simulated IPMSM

Parameter	Value
d-axis inductance L_d	1.03 mH
q-axis inductance L_q	1.31 mH
Resistance R	85 mΩ
Permanent magnet flux linkage K_e	31.2 mWb
Number of pole pairs P	6

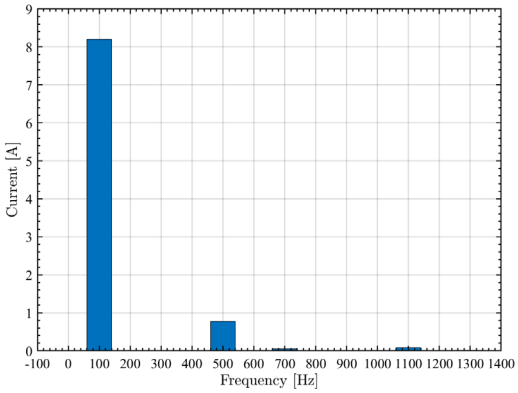

Fig. 2. Amplitude of the simulated motor phase current

Table 2. Simulation results

Loss	with harmonics	without harmonics
Hysteresis loss	3.764 W	3.746 W
Eddy current loss	1.289 W	1.271 W
Total iron loss	5.053 W	5.017 W

experiments were conducted to confirm the possibility that iron loss could be suppressed by improving the current controller. In the simulations, suppressed and non-suppressed motor harmonic currents are set, and the effect of harmonics on iron loss was confirmed, based on the extents of hysteresis and eddy current losses.

2.2 Initial Simulation-based Study The change in the iron loss caused by the harmonic current presence was verified in simulations. JMAG-Designer (JSOL) was used for the electromagnetic field analysis and for the iron loss analysis, while the direct linkage function of the JMAG-Designer and MATLAB & Simulink (MathWorks) was used for simulating the PI current control. The simulated model, which had the same stator and rotor dimensions as the experimental IPMSM, is shown in Fig. 1. This is a 1/6 partial model for simulating the motor size, and the analysis was performed for the setup at 60°. The result was converted into a full model, using periodicity for reducing the calculation scale. 35A360 (JSOL) was used as a material for the electromagnetic steel sheet, while N39UH (Shin-Etsu Chemical) was used as a material for the magnet.

The parameters of this model are listed in Table 1. The values of the residual flux density and coercivity of the magnets in the simulation were adjusted, so that the permanent magnet flux linkage K_e matched that of the experimental motor.

First, the dq-axis current of the simulated motor model was controlled by the PI controller, including the PWM inverter model of the Simulink model. The phase current and typical order harmonics ($n = 5, 7, 11, 13$) in the steady state were recorded. As simulation conditions, the q-axis current was set to 10 A and the d-axis current was set to −0.892 A according to MTPA, as follows [13]:

$$i_{d\,ref} = \frac{K_e}{2(L_q - L_d)} - \sqrt{\frac{K_e^2}{4(L_q - L_d)^2} + i_{q\,ref}^2} \cdots\cdots (1)$$

Iron loss was simulated using the JMAG-Designer. To make the simulation time realistic, the inverter model was not considered in the simulations of iron loss, and the phase current values in the steady state were used to avoid calculating the loss in the transient state. The algorithm for calculating iron loss in the JMAG-Designer included the hysteresis loss calculation algorithm using the play hysteron model, and the eddy current loss calculation algorithm using the homogenization method.

The rotation speed was set to 1000 rpm. The amplitudes of the different components of the phase current, including the harmonics set under this condition, are shown in Fig. 2. The trend of the iron loss caused by the presence of harmonics was investigated by comparing the motor current and an ideal current source.

Table 2 shows the results for iron loss, with and without harmonics. The iron loss values were averaged over a period of the electric angle. These results confirm that removing the harmonic current reduces the hysteresis loss and the eddy current loss, and the overall iron loss is reduced by approximately 0.71%, compared with the case in which the harmonic current is included. Therefore, RPTC, which suppresses the harmonic current, is expected to be effective in reducing iron loss.

3. Overview of the RPTC [7][8]

3.1 Plant Model of the IPMSM The IPMSM model for the dq-coordinate system is shown in Fig. 3. The different parameters are explained in Table 3. In this study, a perfect tracking controller and a PI controller were designed on the dq-coordinate. The dq axis voltage equation is expressed as follows:

$$\begin{bmatrix} v_d \\ v_q \end{bmatrix} = \begin{bmatrix} R + sL_d & -\omega_e L_q \\ \omega_e L_d & R + sL_q \end{bmatrix} \begin{bmatrix} i_d \\ i_q \end{bmatrix} + \begin{bmatrix} 0 \\ \omega_e K_e \end{bmatrix} \cdots\cdots\cdots (2)$$

Because the dq-axis current has coupling terms, decoupling control is widely used. To eliminate the coupling terms, the dq-voltages are calculated as follows:

$$v_d = v_d' - \omega_e L_q i_q, \quad \cdots\cdots\cdots\cdots\cdots\cdots\cdots\cdots (3)$$
$$v_q = v_q' + \omega_e (L_d i_d + K_e). \quad \cdots\cdots\cdots\cdots\cdots\cdots\cdots\cdots (4)$$

State variables are defined as the dq-axis current, and inputs are defined as the decoupled dq-axis voltage. The

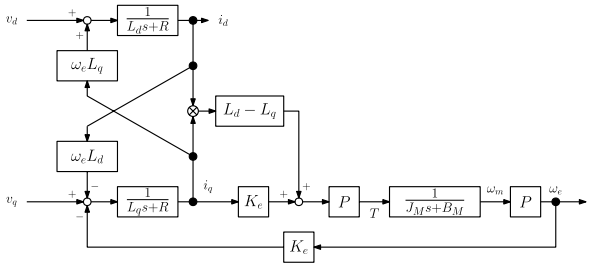

Fig. 3. Block diagram of the IPMSM model

Table 3. Parameters of the IPMSM and their interpretation

Parameter	Meaning
v_d, v_q	dq-axis voltage
i_d, i_q	dq-axis current
L_d, L_q	dq-axis inductance
R	Resistance
K_e	Permanent-magnet flux linkage
P	Number of pole pairs
J_M	Inertia
B_M	Viscous friction coefficient
ω_m	Mechanical angular velocity
ω_e	Electric angular velocity

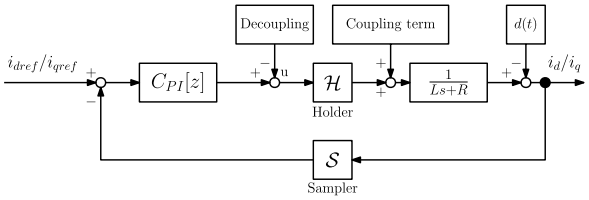

Fig. 4. General current PI control

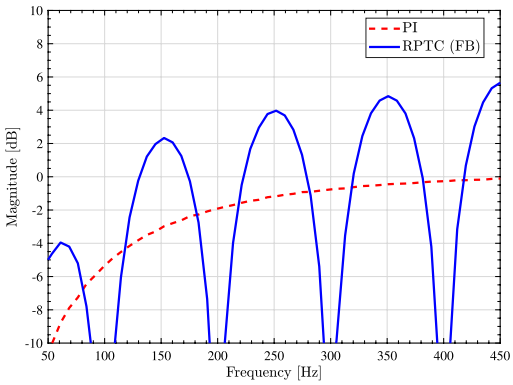

Fig. 5. Sensitivity function of the PI controller and feedback RPTC

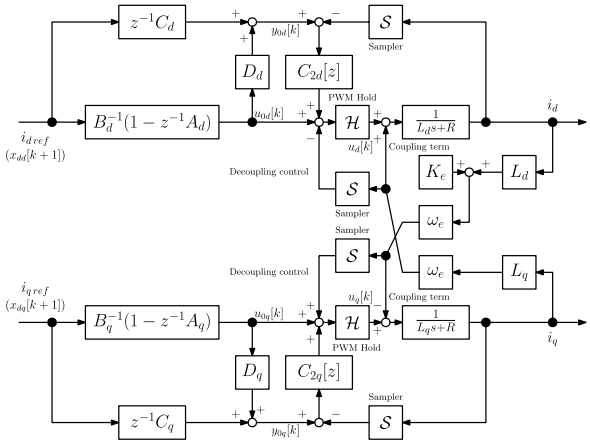

Fig. 6. Block diagram of the PTC (dq-axis current)

continuous-time state equation and the output equation of the IPMSM are expressed as follows:

$$\dot{\boldsymbol{x}}(t) = A_c\boldsymbol{x}(t) + B_c\boldsymbol{u}(t), \quad \cdots\cdots (5)$$

$$\boldsymbol{y}(t) = C_c\boldsymbol{x}(t) + D_c\boldsymbol{u}(t), \quad \cdots\cdots (6)$$

where

$$\boldsymbol{x}(t) = \begin{bmatrix} i_d(t) \\ i_q(t) \end{bmatrix}, \quad \boldsymbol{u}(t) = \begin{bmatrix} v'_d(t) \\ v'_q(t) \end{bmatrix}, \quad \cdots\cdots (7)$$

$$\begin{cases} A_c = \begin{bmatrix} -\frac{R}{L_d} & 0 \\ 0 & -\frac{R}{L_q} \end{bmatrix}, B_c = \begin{bmatrix} \frac{1}{L_d} & 0 \\ 0 & \frac{1}{L_q} \end{bmatrix}, \\ C_c = \begin{bmatrix} 1 & 0 \\ 0 & 1 \end{bmatrix}, D_c = O. \end{cases} \quad \cdots\cdots (8)$$

3.2 Design of the Feedback Controller In general, a PI controller is used for current control. The control system that was used in the present study is illustrated in Fig. 4. The current PI controller $C_{PI}(s)$ was designed using the pole zero cancellation method and is given as follows:

$$C_{PI}(s) = \frac{Ls+R}{\tau s}. \quad \cdots\cdots (9)$$

τ is often set to approximately 10 times the control period. $C_{PI}[z]$ is the discretized $C_{PI}(s)$. Considering Eq. (5), and Eq. (6), the transfer function from the reference current $i_{d,q\,ref}$ to the PMSM dq-current $i_{d,q}$ is derived as follows:

$$\frac{i_{d,q}}{i_{d,q\,ref}} = \frac{1}{\tau s+1}. \quad \cdots\cdots (10)$$

Fig. 5 shows the sensitivity function from the output end disturbance ($d(t)$ in Fig. 4) to the output. This figure suggests that the PI controller is not able to suppress disturbances such as harmonics, which have higher frequency components than the bandwidth of the controller; thus, the tracking error remains. Since there is a limit to extending the bandwidth of the PI controller, harmonics suppression by the RPTC focusing on the periodicity of disturbance was investigated.

3.3 PTC The block diagram of the PTC on the dq-axis is shown in Fig. 6. Subscripts d and q indicate that each coefficient and variable are calculated on its axis. The PTC system has a feedforward controller and a feedback controller ($C_2[z]$). The feedforward controller is a stable inverse system that achieves zero error to the target value at the sampling points [6]. For the n-th order plant model, it is necessary to switch the control input n times. In the case of this IPMSM model, the plant is a first-order model and is controlled by a single-rate controller.

To design the feedforward controller, the state and output equations in Eq. (5) and Eq. (6) are discretized using the PWM hold [14]. In contrast to other holders based on the averaging approximation that assumes that the inverter can output arbitrary voltages, PWM hold is a discretization based on a PWM pulse consisting of the inverter voltage $\pm E$ [V] and 0 [V]. The control input $u[k]$ is the inverter's ON time. Therefore, the PWM hold is more appropriate than the zero-order

hold for instantaneous value control [15][16]. The discrete time state and output equation of the IPMSM based on the PWM hold are expressed as follows:

$$x[k+1] = Ax[k] + Bu[k], \cdots\cdots\cdots\cdots\cdots\cdots (11)$$
$$y[k] = Cx[k] + Du[k]. \cdots\cdots\cdots\cdots\cdots\cdots (12)$$

A, B, C, and D are calculated using Eq. (13). T_u is the control input period. E is the DC power supply voltage of a 3-phase inverter.

$$A = e^{A_c T_u},\ B = e^{A_c T_u/2} B_c E,\ C = C_c,\ D = D_c. \cdots (13)$$

From Eq. (11), and Eq. (12), the stable inverse model, and the nominal output are expressed as Eq. (14), and Eq. (15).

$$u_0[k] = B^{-1}(1 - z^{-1}A)x_d[k+1], \cdots\cdots\cdots\cdots (14)$$
$$y_0[k] = z^{-1}Cx_d[k+1] + Du_0[k]. \cdots\cdots\cdots\cdots (15)$$

In reality, disturbances and modeling errors occur. However, these can be suppressed by a feedback controller $C_2[z]$, and the tracking performance is improved by the feedforward controller. $C_2[z]$ denotes the discretized PI controller.

3.4 RPTC

3.4.1 Feedback RPTC (FB RPTC) In this section, feedback type RPTC based on the internal model principle is described. The block diagram of the FB RPTC on the dq-axis is shown in Fig. 7. The decoupling control and coupling terms are the same as those in Fig. 6. The RPTC system has a periodic signal generator (PSG). The PSG records the periodic disturbance in memory and uses it for compensation [8][17].

The memory size is defined as N_d. The memory size N_d is expressed by Eq. (16) using a tracking error period T_d and a control period T_s.

$$N_d = \frac{T_d}{T_s}. \cdots\cdots\cdots\cdots\cdots\cdots\cdots\cdots\cdots\cdots (16)$$

For the implementation, a low-pass filter Q with no phase delay is applied to the compensation signal, for removing the sensor noise. The low-pass filter is expressed as follows:

$$r_f[k] = Qr[k] = \frac{z + \gamma + z^{-1}}{\gamma + 2} r[k], \cdots\cdots\cdots\cdots (17)$$

where $r_f[k]$ is the filter output, $r[k]$ is the PSG output, and γ is the design parameter of the filter. In this experiment, γ was set to 2, and the cutoff frequency of the filter was 1.8 kHz [8][18].

In this study, T_s was set to 0.1 ms, and τ of the PI controller mentioned in Section 3.2 was set to $10T_s = 1$ ms. $C_2[z]$ was obtained from $C_{PI}(s)$, using the Tustin transformation. The period of the transformation wass T_s. The RPTC has PSG and $C_2[z]$. In the experiment, the conventional method only had this feedback controller.

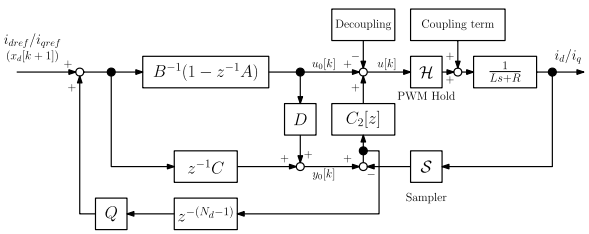

Fig. 7. Block diagram of the feedback RPTC (dq-axis current)

The RPTC has a PSG that adds the compensation signal for the periodic tracking error to the current command and the feedforward controller of the PTC that achieves zero error to the target value one sample ahead at each sampling point. Therefore, the RPTC can suppress harmonics that cannot be suppressed in the bandwidth of the PI controller. The sensitivity function from the output end disturbance $d(t)$ to the output for the basic configuration of the FB RPTC without the low-pass filter is shown in Fig. 5. In Fig. 5, the fundamental frequency of the harmonic disturbance to be suppressed was set to 100 Hz. This result shows that the RPTC strongly suppresses the harmonics. However, the FB RPTC based on the internal model principle exhibits some problems, such as a deterioration of the suppression characteristics of other order harmonics and disturbance relearning when the speed changes. To solve these problems, a feedforward RPTC was also considered in this study.

3.4.2 Feedforward RPTC (FF RPTC) RPTC can realize a feedforward controller by switching the compensation signal of the PSG [7]. A block diagram of the RPTC with switches is shown in Fig. 8. By turning ON or OFF two switches, feedforward type error compensation is performed. Switch 1 is turned on to record errors in the memory during one period of the periodic disturbance after reaching the steady state. After recording, switch 1 is turned off

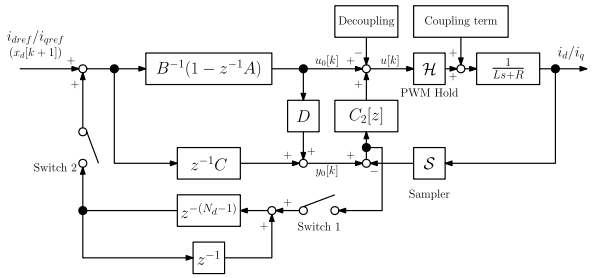

Fig. 8. Block diagram of the RPTC with switches

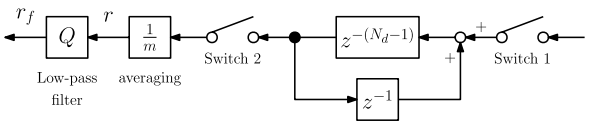

Fig. 9. Block diagram of the PSG

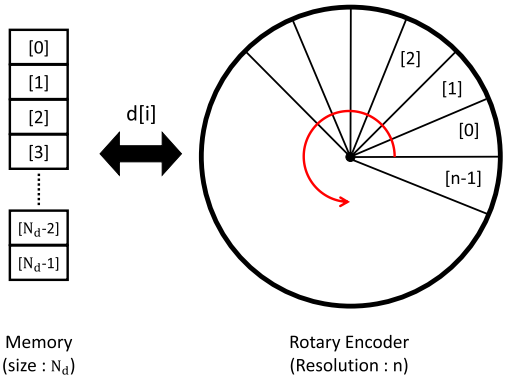

Fig. 10. PSG for handling speed variations

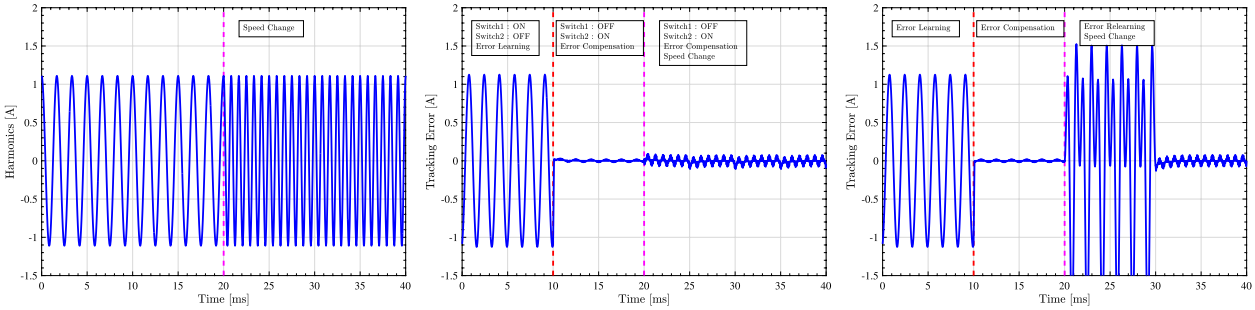

(a) Harmonics with speed variations (b) Tracking error (feedforward RPTC) (c) Tracking error (feedback RPTC)

Fig. 11. Tracking errors, for the simulated FF and FB RPTC

and switch 2 is turned on, to compensate for the tracking error caused by the periodic disturbance as a feedforward controller. Feedforward compensation has the advantage of not exacerbating the inter-harmonics.

Theoretically, it is sufficient to record the tracking error for one period. However, tracking errors were recorded for several periods and averaged to remove the asynchronous components. The compensation signal is then passed through the low-pass filter Q. In this study, the average number of times m was set to 10. A more detailed block diagram of the PSG is shown in Fig. 9.

In addition, the compensation signal recorded in the memory is linked to the position information of the rotary encoder, for handling speed variations [17]. Assuming that the main cause of harmonics is the distortion of the flux linkage caused by the motor structure, the appearance of harmonics is considered to be highly dependent on the position of the rotor. Therefore, suppression of harmonics is possible even for speed variations by referring to the encoder information and recalling the compensation signal in the memory, as shown in Fig. 10.

The simulation showed the difference in disturbance suppression between the FF RPTC and FB RPTC, with respect to speed variations. The disturbance current simulating the 6th-order harmonics was added to the output end of the control system in Fig. 7 and Fig. 8, and the tracking errors are shown in Fig. 11. Because the speed doubled at 20 ms, the frequency of the harmonics also doubled. At this time, the FB RPTC had to relearn the tracking error, but the FF RPTC provided the compensation signal generated in the first error-recording step as the feedforward signal referring to the encoder position. This system enabled instantaneous error compensation.

4. Experiment

4.1 Experimental Setup and Conditions The experimental setup is shown in Fig. 12, and the parameters of the IPMSM used in this experiment are listed in Table 4. Because this is a single-rate control, T_u and T_s were the same value and set to 0.1 ms.

As the driving conditions, the q-axis current command was set to $i_{q\,ref} = 10\,\mathrm{A}$, and the d-axis current command was set to $i_{d\,ref} = -1.86\,\mathrm{A}$ according to the MTPA condition in Eq. (1). The rotation speed was maintained at 1000 rpm by a load servo motor. Thus, the electrical angular frequency was 100 Hz. The fundamental frequency of the tracking error to be suppressed by the RPTC was set as the mechanical

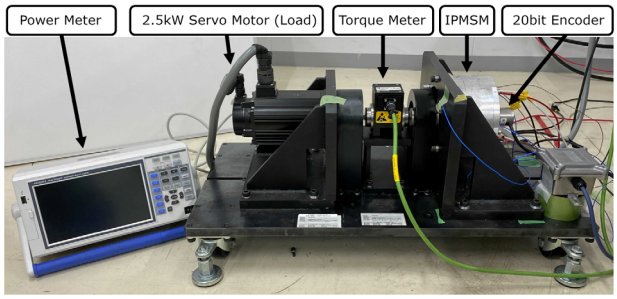

Fig. 12. Experimental setup

Table 4. Parameters of the experimental IPMSM

Parameter	Value
d-axis inductance L_d	0.613 mH
q-axis inductance L_q	1.21 mH
Resistance R	85.6 mΩ
Permanent magnet flux linkage K_e	31.2 mWb
Pole pairs P	6
Supply voltage V_{dc}	100 V
Carrier frequency F_s	10 kHz
Control period T_s	0.1 ms
Memory size N_d	600

angular frequency. Thus, the memory size N_d was 600 from Eq. (16). This is because the mechanical angular velocity component caused by the encoder eccentricity or vibration was confirmed on the dq-axis.

In the loss measurement experiment, iron loss was calculated by subtracting the IPMSM output, copper loss, and mechanical loss from the input power, as follows:

$$P_{ir} = P_{in} - P_{out} - P_{co} - P_{me}, \cdots\cdots\cdots\cdots\cdots\cdots (18)$$

where P_{in} is the input power, P_{out} is the output power, P_{co} is the copper loss, P_{ir} is the iron loss, and P_{me} isthe mechanical loss. Mechanical loss is considered to be caused by friction and other factors.

The power meter measured the input power and the phase current. Copper loss in this study was calculated from the phase current and winding resistance measured in advance, as follows:

$$P_{co} = I_{u\,rms}^2 R_u + I_{v\,rms}^2 R_v + I_{w\,rms}^2 R_w, \cdots\cdots\cdots\cdots (19)$$

where $I_{u\,rms}$, $I_{v\,rms}$ and $I_{w\,rms}$ are the phase currents. R_u, R_v and R_w are the resistances of the windings.

The output of the IPMSM was calculated from the torque measured by the torque meter and the rotation speed measured by the encoder, as follows:

Table 5. Experimental temperature and phase resistance

Parameter	Value
Initial winding temperature T_{STi}	20.3 °C
U phase resistance $R_u(T_{STi})$	86.3 mΩ
V phase resistance $R_v(T_{STi})$	88.1 mΩ
W phase resistance $R_w(T_{STi})$	86.7 mΩ
Temperature coefficient α	3.92×10^{-3}

$$P_{out} = \tau_m \omega_m, \cdots\cdots\cdots\cdots\cdots\cdots\cdots\cdots\cdots\cdots \quad (20)$$

where τ_m denotes the motor torque. The mechanical loss P_{me} was also calculated using the measured torque and rotation speed. This mechanical loss was measured beforehand by rotating the rotor of the IPMSM without magnets. The rotation speed was maintained at 1000 rpm by the load servo motor.

A power meter PW3390 (HIOKI), which was able to measure electric power with an accuracy of 0.01 W, was used. The torque meter TMB307/411 (MAGTROL), which could measure up to 10 Nm torque with an accuracy of ±0.15% was used.

Measurements of the input power, output power, and different losses were conducted separately using the PI control and RPTC, for 5 s. These procedures were performed 12 times. The results for P_{ir} were compared for the same set, and the averages over 10 sets, excluding the maximum and minimum differences of P_{ir}, are reported as loss reduction results.

Thermocouple thermometers were attached to the bearing and windings of the IPMSM. Because the mechanical loss was expected to vary with temperature, the bearing temperature was maintained as stable as possible, for minimizing the variation in the mechanical loss. Therefore, the mechanical loss measured beforehand was assumed to be constant in all sets of experiments. In addition, more accurate copper loss results were calculated by correcting the winding resistance of each phase, as follows [19]:

$$R(T_{ST}) = R(T_{STi})\{1 + \alpha(T_{ST} - T_{STi})\}, \cdots\cdots\cdots\cdots \quad (21)$$

where T_{ST} is the winding temperature, T_{STi} is the initial winding temperature and α is the temperature coefficient of the copper resistance (20.3°C). The experimental conditions are listed in Table 5.

4.2 Experimental Results Fig. 13 and Fig. 14 show the fast Fourier transform (FFT) results of current control for the PI control, the FF RPTC, and the FB RPTC. In addition, Table 6 lists the amplitudes of typical harmonics. The results confirm that the FF and FB RPTCs suppress the 6th and 12th order harmonics significantly. For determining the impact of the FF RPTC handling speed variations, the harmonic components at 1200 rpm were investigated using the compensation signal recorded at 1000 rpm. Fig. 15 shows the FFT results for the current PI control and for the FF RPTC, at 1200 rpm. Table 7 lists the amplitudes of typical harmonics.

According to the results, the FF RPTC does not inherently worsen the inter-order harmonics, but some parts of the harmonics are worsened, as shown in Fig. 13, Fig. 14 and Fig. 15.This error is owing to the modeling error of the feedforward controller. However, the FF RPTC strongly suppresses the typical harmonic components, such as the 6th order, and is expected to be useful for a broader range of conditions than the FB RPTC, owing to its performance on handling speed variations.

Table 6. Current amplitude of dq-axis harmonics (average)

Current amplitude	Fundamental	The 6th harmonic	The 12th harmonic
id_{PI}	1.86 A	615 mA	101 mA
$id_{FF\,RPTC}$	1.86 A	210 mA	99.6 mA
$id_{FB\,RPTC}$	1.86 A	45.7 mA	37.0 mA
iq_{PI}	10.0 A	495 mA	20.3 mA
$iq_{FF\,RPTC}$	10.0 A	150 mA	13.2 mA
$iq_{FB\,RPTC}$	10.0 A	23.7 mA	2.51 mA

Table 7. Current amplitude of dq-axis harmonics at 1200 rpm (average)

Current amplitude	Fundamental	The 6th harmonic	The 12th harmonic
id_{PI}	1.86 A	731 mA	77.7 mA
$id_{FF\,RPTC}$	1.86 A	242 mA	74.0 mA
iq_{PI}	10.0 A	576 mA	10.5 mA
$iq_{FF\,RPTC}$	10.0 A	233 mA	10.1 mA

Table 8. Efficiency and ratio of loss to input power (average)

Efficiency and Loss	PI	FF RPTC	FB RPTC
Efficiency	95.09%	95.18%	95.19%
Copper loss P_{co}	3.33%	3.29%	3.28%
Iron loss P_{ir}	0.37%	0.32%	0.32%

Table 8 lists the efficiency and loss ratios. Each value was normalized by the input power of the IPMSM. These values are averages calculated over 10 sets of experimental results.

Because the amount of iron loss is small, it is affected by the measurement error of the torque meter. Therefore, the maximum and minimum values of the results are shown in Fig. 16, and Fig. 17 as the error range. As a result, the iron loss reduction effect of the RPTC was confirmed by repeating the experiment and averaging the results. In terms of the efficiency and the loss relative to the input power, it was confirmed that the FF RPTC improved the driving efficiency by 0.09% and FB RPTC improved it by 0.1%, compared with the PI controller. The iron loss of the FF and FB RPTCs was reduced to approximately 86.0% of the PI controller's iron loss.

The simulation results in Section 2 confirmed that the suppressing the harmonic current reduces iron loss, and this experiment also showed that suppression of the 6th and 12th order harmonics on the dq-axis reduced the IPMSM loss. The differences in iron loss between the PI and FF RPTC and between the PI and FB RPTC were significant. However, the difference in iron loss between the FF RPTC and FB RPTC was slight. These results indicate that the current disturbance suppression at high frequencies is important for reducing iron loss and for improving efficiency. It can be said that the FF RPTC can handle speed variations and exhibits almost the same efficiency improvement as in the case of the feedback harmonics suppression based on the internal model principle.

4.3 Loss Simulation using Actual Phase Current Data Because several measuring instruments were used in this experiment, there is variation in the loss results as shown in Fig. 16, and Fig. 17. Therefore, the actual phase current data of the PI control and RPTC were used for additional verification by the JMAG-Designer simulation.

The actual phase current data were recorded using the current probe TCP0020 (Tektronix). The measurement range of

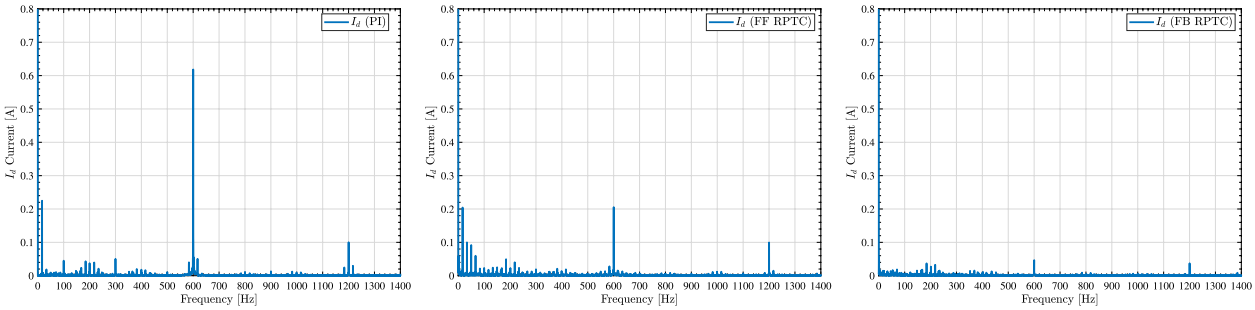

(a) Spectrum of I_d (PI) (b) Spectrum of I_d (FF RPTC) (c) Spectrum of I_d (FB RPTC)

Fig. 13. Comparison of d-axis harmonics (left: PI, center: FF RPTC, right: FB RPTC)

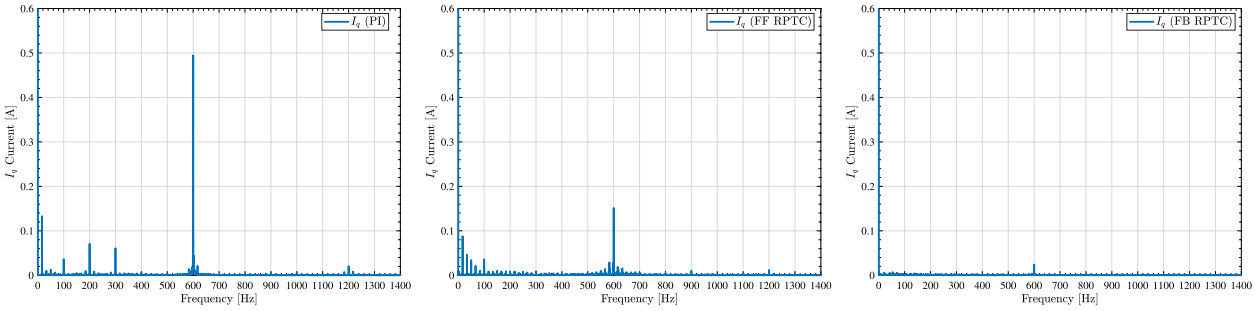

(a) Spectrum of I_q (PI) (b) Spectrum of I_q (FF RPTC) (c) Spectrum of I_q (FB RPTC)

Fig. 14. Comparison of q-axis harmonics (left: PI, center: FF RPTC, right: FB RPTC)

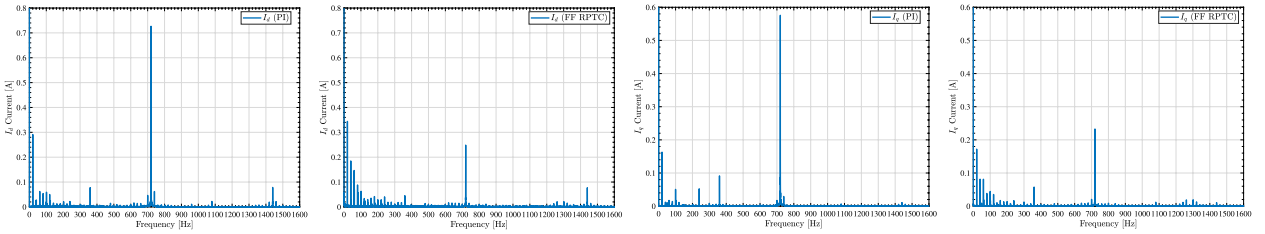

(a) Spectrum of I_d (PI 1200 rpm) (b) Spectrum of I_d (FF RPTC 1200 rpm) (c) Spectrum of I_q (PI 1200 rpm) (d) Spectrum of I_q (FF RPTC 1200 rpm)

Fig. 15. Comparison of PI and FF RPTC dq-axis harmonics (1200 rpm with learning signal at 1000 rpm)

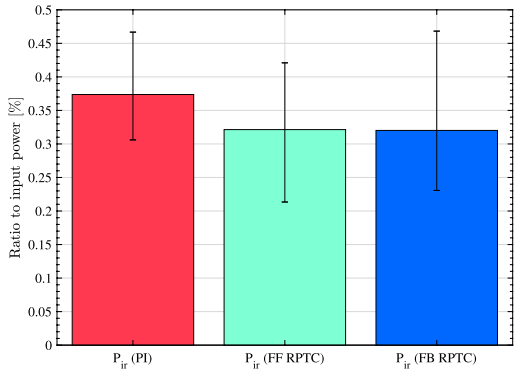

Fig. 16. Ratio of iron loss, and range of errors

the current probe was set to 20 A. These data were applied using the current source in the IPMSM simulation model shown in Fig. 1, and the rotation speed was set to 1000 rpm.

Table 9 shows the efficiency and the loss ratio for the simulation using current data. Owing to the slight differences in the input power and output for each controller, each value was calculated as a ratio to the input power. Since this simulation did not capture the mechanical loss, the input power was calculated as follows, using the measurement mechanical loss P_{me}:

$$P'_{in} = P'_{out} + P'_{co} + P'_{ir} + P_{me}, \cdots\cdots\cdots\cdots\cdots\cdots \quad (22)$$

where P'_{in}, P'_{out}, P'_{co}, and P'_{ir} are analytical values. The iron loss calculation algorithm used in this simulation was the same as that described in Section 2.

In terms of the efficiency and the loss as a ratio to the input power, the results in Table 9 confirm that the FF RPTC improved the driving efficiency by 0.07% and FB RPTC improved it by 0.13%, compared with the PI controller. Considering iron loss in more detail, the FF and FB RPTC reduced 3.0 $\sim$ 3.2% of the iron loss caused by the PI controller. The actual phase current data were obtained from the experiments in Section 4.2. As shown in Fig. 13, Fig. 14, and Table 6, the harmonics of the phase currents of the FF and FB RPTC were suppressed, and the JMAG simulation using these data also showed the trend for the iron loss reduction, owing to the RPTC. Comparing the results in Tables 8 and 9, the trend of the difference in iron loss between the PI and the FF RPTC, and between the PI and the FB RPTC was significant, and the difference in iron loss between the FF RPTC and the FB RPTC was slight, which was also consistent between the experimental and simulation results. Therefore, the simulation results also support the experimental observations

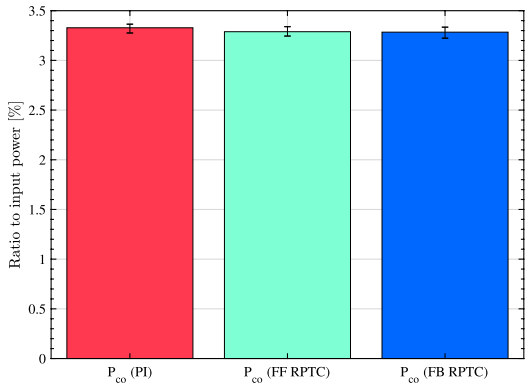

(a) Overall view.

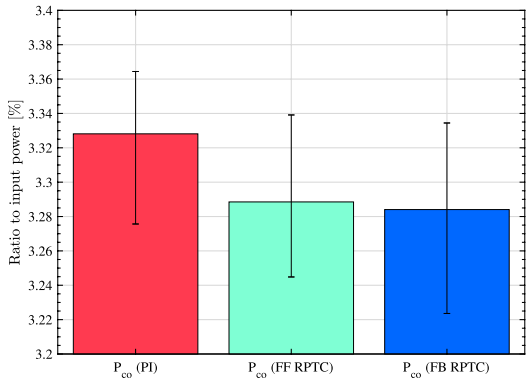

(b) Magnified view.

Fig. 17. Ratio of copper loss, and range of errors

Table 9. Efficiency and ratio of loss to input power (using actual current data)

Efficiency and Loss	PI	FF RPTC	FB RPTC
Efficiency	94.02%	94.09%	94.15%
Copper loss P'_{co}	3.23%	3.19%	3.15%
Iron loss P'_{ir}	1.61%	1.56%	1.57%

that changing the current controller from the PI to the RPTC effectively reduces losses.

5. Conclusion

In this paper, the application of the RPTC to current control was proposed, for reducing the iron loss of IPMSMs. The harmonics of an IPMSM increase the iron loss and decrease the motor's driving efficiency. Because the harmonics can be regarded as a periodic disturbance, they can be suppressed by the RPTC, which is a repetitive control based on the PTC. In the RPTC, the harmonics of the fundamental frequency are recorded as errors and compensated by the periodic signal generator, for suppressing harmonics and reducing iron loss.

The first simulation results showed that iron loss was reduced when the harmonic current was eliminated. The experimental results also showed that the iron loss of the FF and FB RPTC was reduced to 86.0% of the PI controller's iron loss. The FF RPTC improved the driving efficiency by 0.09%, while the FB RPTC improved it by 0.1%, compared with the PI controller. Furthermore, an additional experiment was conducted by the simulation using actual current data. The simulation results showed that the FF and the FB RPTC reduced 3.0 ∼ 3.2% of iron loss caused by the PI controller, and the FF RPTC improved the driving efficiency by 0.07%, while the FB RPTC improved it by 0.13%. The reduction of iron loss and the improvement of efficiency owing to the suppression of harmonics were confirmed by both experimental results and simulation results.

Regarding the different RPTC schemes, according to our experimental results, the FF RPTC still exhibited the tracking error derived from the modeling error, while the FB RPTC almost suppressed the harmonics in the steady state. However, in terms of the iron loss and drive efficiency, these two methods exhibited similar performances. Based on these results, the FF RPTC performed better than the PI control in terms of efficiency; in addition, it could handle speed variations.

There is a research that shows the possibility of improving efficiency when the harmonic current commands are set to other than 0 A [20]. Verification of changes in the iron loss and total loss for the PMSM when the harmonic current is actively controlled is a topic for future work. In addition, the relationship between harmonic control and motor drive performance has conventionally been studied from the perspective of the torque ripples [21][22]. In the future, it will be necessary to consider the three elements, namely the harmonic control, the drive efficiency, and the torque ripples.

References

(1) T. Inoue, Y. Inoue, S. Morimoto, and M. Sanada: "Maximum Torque per Ampere Control of a Direct Torque-Controlled PMSM in a Stator Flux Linkage Synchronous Frame", *IEEE Transactions on Industry Applications*, Vol.52, No.3, pp.2360–2367 (2016)

(2) Q. Guo, C. Zhang, L. Li, J. Zhang, and M. Wang: "Maximum efficiency per torque control of permanent-magnet synchronous machines", *IEEE Transactions on Industrial Electronics*, Vol.62, No.4, pp.2135–2143 (2015)

(3) H. Zhang, M. Dou, and J. Deng: "Loss-minimization strategy of nonsinusoidal back EMF PMSM in multiple synchronous reference frames", *IEEE Transactions on Power Electronics*, Vol.35, No.8, pp.8335–8346 (2020)

(4) A. Balamurali, G. Feng, A. Kundu, H. Dhulipati, and N.C. Kar: "Noninvasive and Improved Torque and Efficiency Calculation Toward Current Advance Angle Determination for Maximum Efficiency Control of PMSM", *IEEE Transactions on Transportation Electrification*, Vol.6, No.1, pp.28–40 (2020)

(5) J. Lee, Y.C. Kwon, and S.K. Sul: "Experimental Identification of IPMSM Flux-Linkage Considering Spatial Harmonics for High-Accuracy Simulation of IPMSM Drives", *2018 IEEE Energy Conversion Congress and Exposition, ECCE 2018*, pp.5804–5809 (2018)

(6) H. Fujimoto, Y. Hori, and A. Kawamura: "Perfect tracking control based on multirate feedforward control with generalized sampling periods", *IEEE Transactions on Industrial Electronics*, Vol.48, No.3, pp.636–644 (2001)

(7) T. Nakai and H. Fujimoto: "Harmonic Current Suppression Method of PMSM Based on Repetitive Perfect Tracking Control", *IECON 2007 - 33rd Annual Conference of the IEEE Industrial Electronics Society*, pp.1049–1054 (2007)

(8) H. Fujimoto and T. Takemura: "High-precision control of ball-screw-driven stage based on repetitive control using n-times learning filter", *IEEE Transactions on Industrial Electronics*, Vol.61, No.7, pp.3694–3703 (2014)

(9) K. Yamazaki and A. Abe: "Loss investigation of interior permanent-magnet motors considering carrier harmonics and magnet eddy currents", *IEEE Transactions on Industry Applications*, Vol.45, No.2, pp.659–665 (2009)

(10) H. Nam, K.H. Ha, J.J. Lee, J.P. Hong, and G.H. Kang: "A study on iron loss analysis method considering the harmonics of the flux density waveform using iron loss curves tested on epstein samples", *IEEE Transactions on Magnetics*, Vol.39, No.3 I, pp.1472–1475 (2003)

(11) K. Narita, H. Sano, T. Yamada, R. Akaki, and M. Aoyama: "An Accurate Iron Loss Analysis Method Based on Finite Element Analysis Considering Dynamic Anomalous Loss", *2018 IEEE Energy Conversion Congress and Exposition, ECCE 2018*, no. ohm m, pp.4309–4314 (2018)

(12) G. Liu, M. Liu, Y. Zhang, H. Wang, and C. Gerada: "High-speed permanent magnet synchronous motor iron loss calculation method considering multiphysics factors", *IEEE Transactions on Industrial Electronics*, Vol.67, No.7,

pp.5360–5368 (2020)
(13) S. Morimoto, M. Sanada, and Y. Takeda: "Wide-Speed Operation of Interior Permanent Magnet Synchronous Motors with High-Performance Current Regulator", *IEEE Transactions on Industry Applications*, Vol.30, No.4, pp.920–926 (1994)
(14) A. Kawamura, H. Fujimoto, and T. Yokoyama: "Survey on the real time digital feedback control of PWM inverter and the extension to multi-rate sampling and FPGA based inverter control", *IECON Proceedings (Industrial Electronics Conference)*, No.1, pp.2044–2051 (2007)
(15) K. Sakata and H. Fujimoto: "Perfect tracking control of servo motor based on precise model with PWM hold and current loop", *Fourth Power Conversion Conference-NAGOYA, PCC-NAGOYA 2007 - Conference Proceedings*, pp.1612–1617 (2007)
(16) T. Miyajima, H. Fujimoto, and M. Fujitsuna: "Control method for IPMSM based on PTC and PWM hold model in overmodulation range—Study on robustness and comparison with anti-windup control—", *2010 IEEE Energy Conversion Congress and Exposition, ECCE 2010 - Proceedings*, pp.2844–2850 (2010)
(17) T. Nakai and H. Fujimoto: "Harmonic current suppression method of SPM motor based on repetitive perfect tracking control with speed variation", *IECON Proceedings (Industrial Electronics Conference)*, No.2, pp.1210–1215 (2008)
(18) K.K. Chew and M. Tomizuka: "Digital Control of Repetitive Errors in Disk Drive Systems", *IEEE Control Systems Magazine*, Vol.10, No.1, pp.16–20 (1990)
(19) H. Iwata, K. Ohishi, Y. Yokokura, Y. Okada, Y. Ide, D. Kuraishi, and A. Takahashi: "Robust Estimation Method for Stator Temperature Based on Voltage Disturbance Observer Autotuning Resistance for SPMSM", *IEEJ Journal of Industry Applications*, Vol.9, No.4, pp.341–350 (2020)
(20) K. Yoshimoto and Y. Kitajima: "A Novel Harmonic Current Control for IPMSMs", *The 2005 International Power Electronics Conference A Multi-Mode Charging Circuit for Rechargeable Batteries*, pp.1569–1574 (2005)
(21) K. Nakamura, H. Fujimoto, and M. Fujitsuna: "Torque ripple suppression control for PM motor with current control based on PTC", *2010 International Power Electronics Conference - ECCE Asia -, IPEC 2010*, No.1, pp.1077–1082 (2010)
(22) N. Nakao, K. Tobari, T. Sugino, Y. Ito, M. Mishima, and D. Maeda: "Torque ripple suppression control for PMSMs using feedforward compensation and online parameter estimation", *IEEJ Journal of Industry Applications*, Vol.10, No.4, pp.497–505 (2021)

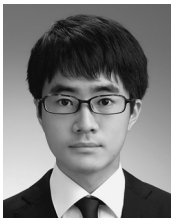

Yuhiro Inagaki (Student Member) received the B.E. degree from Waseda University in 2020. He is currently working toward the M.E. degree in Department of Electrical Engineering and Information Systems, Graduate School of Engineering, the University of Tokyo. His interests are in motor drive, motion control.

Masahiro Mae (Student Member) received the B.E. and M.S. degrees from The University of Tokyo in 2018 and 2020, respectively. He is currently working towards the Ph.D. degree in the Department of Electrical Engineering and Information Systems, Graduate School of Engineering, The University of Tokyo. He is also a research fellow (DC2) of Japan Society for the Promotion of Science from 2021. His research interests are in control engineering, precision motion control, multirate control, and multi-input multi-output systems. He is a student member of the Institute of Electrical and Electronics Engineers and the Society of Instrumental and Control Engineers.

Osamu Shimizu (Member) received the B.S. and M.S. degrees in Faculty of Environment and Information Studies from Keio University, Japan in 2007 and 2009, respectively. He worked as an associate at Toyota Motor Corporation, Sim-Drive Co., Ltd., Honda R & D Co., Ltd. in 2009–2017. He received the Ph.D. degree in the Department of Media and Governance from Keio University in Japan. He joined as assistant professor at Nagoya University in 2017. From 2018. He joined Graduate School of Frontier Science at University of Tokyo as a project assistant professor and became a project lecturer from year 2021. His interests are in design and control of electric vehicle driving system and WPT system. He is a member of IEEE, IEE and the Society of Automotive Engineers of Japan.

Sakahisa Nagai (Member) received the B.E., M.E., and Ph.D. degrees in electrical and computer engineering from Yokohama National University, Kanagawa, Japan, in 2014, 2016, and 2019, respectively. He was a JSPS fellowship for Young Scientists from 2018 to 2019. In 2019, he joined the University of Tokyo, Chiba, Japan, as a project assistant professor. His research interests include sensorless actuation, motion control, wireless power transfer, and power electronics. He is a member of IEEE and IEE Japan.

Hiroshi Fujimoto (Senior Member) received the Ph.D. degree in the Department of Electrical Engineering from the University of Tokyo in 2001. In 2001, he joined the Department of Electrical Engineering, Nagaoka University of Technology, Niigata, Japan, as a research associate. From 2002 to 2003, he was a visiting scholar in the School of Mechanical Engineering, Purdue University, U.S.A. In 2004, he joined the Department of Electrical and Computer Engineering, Yokohama National University, Yokohama, Japan, as a lecturer and he became an associate professor in 2005. He had been an associate professor of the University of Tokyo from 2010 to 2020 and became a professor from year 2021. He received the Best Paper Awards from the IEEE Transactions on Industrial Electronics in 2001 and 2013, Isao Takahashi Power Electronics Award in 2010, Best Author Prize of SICE in 2010, The Nagamori Grand Award in 2016, and First Prize Paper Award IEEE Transactions on Power Electronics in 2016. His interests are in control engineering, motion control, nano-scale servo systems, electric vehicle control, motor drive, visual servoing, and wireless motors. Dr. Fujimoto is a senior member of IEE of Japan and IEEE. He is also a member of the Society of Instrument and Control Engineers, the Robotics Society of Japan, and the Society of Automotive Engineers of Japan. He is an associate editor of IEEE/ASME Transactions on Mechatronics from 2010 to 2014, IEEE Industrial Electronics Magazine from 2006, IEE of Japan Transactions on Industrial Application from 2013, and Transactions on SICE from 2013 to 2016. He is a chairperson of JSAaE vehicle electrification committee from 2014 to 2020 and a past chairperson of IEEE/IES Technical Committee on Motion Control from 2012 to 2013.

Takayuki Miyajima (Member) received the B.S. and M.S. degrees in electrical and computer engineering from Yokohama National University, Japan, in 2009 and 2011, respectively and the Ph.D. degree from the University of Tokyo, Japan in 2014. From April 2014, he has been with DAIKIN INDUSTRIES, Ltd. He works on the development of motor control of air conditioner and hydraulic equipment.

Yoshiki Yasuda (Member) received the B.E. and M.E. degrees from Osaka Prefecture University, Sakai, Japan, in 2002, 2004 respectively. Since 2004, he has been with DAIKIN INDUSTRIES, Ltd. He works on the development of motors for air conditioners and hydraulic equipment.

Akio Yamagiwa (Member) received the B.E. and M.E. degrees from Toyama University, Toyama, Japan, in 1988 and 1990, respectively. From 1990, he has been with DAIKIN INDUSTRIES, Ltd. He works on the development of motors for air conditioners and hydraulic equipment. He was a senior researcher from 2002 to 2011 and has been a chief engineer from 2012. He was general manager of the Technology Research Association of Magnetic Materials for High-Efficiency Motors from 2012 to 2017 and has been a chief researcher from 2018. He received the IEEJ Technical Development Award in 1998. He is a member of IEE of Japan and the Japan Society of Mechanical Engineers.